Letter

Microscopic and stochastic simulations of chemically active droplets

Roxanne Berthin [iD],[*] Jacques D. Fries,[*] Marie Jardat, Vincent Dahirel [iD], and Pierre Illien [iD]

Sorbonne Université, CNRS, Physico-Chimie des Électrolytes et Nanosystèmes Interfaciaux (PHENIX),
4 Place Jussieu, 75005 Paris, France

Biomolecular condensates play a central role in the spatial organization of living matter. Their formation is now well understood as a form of liquid-liquid phase separation that occurs very far from equilibrium. For instance, they can be modeled as active droplets, where the combination of molecular interactions and chemical reactions result in microphase separation. However, so far, models of chemically active droplets are spatially continuous and deterministic. Therefore, the relationship between the microscopic parameters of the models and some crucial properties of active droplets (such as their polydispersity, their shape anisotropy, or their typical lifetime) is yet to be established. In this work, we address this question computationally, using Brownian dynamics simulations of chemically active droplets: the building blocks are represented explicitly as particles that interact with attractive or repulsive interactions, depending on whether they are in a droplet-forming state or not. Thanks to this microscopic and stochastic view of the problem, we reveal how driving the system away from equilibrium in a controlled way determines the fluctuations and dynamics of active emulsions.

Introduction. The formation of biomolecular condensates is a central feature of the spatial organization of living matter at the subcellular and subnuclear levels, and plays a key role in the regulation of multiple metabolic processes [1,2]. During recent years, a significant research effort has been devoted to understanding the physical and chemical mechanisms that govern the formation and the dynamics of these membraneless organelles, both from experimental and theoretical points of view. The now widely spread picture is that of a form of liquid-liquid phase separation that takes place very far from thermodynamic equilibrium, and that typically results in the selection of a well-defined size for the condensates [3–6].

From a thermodynamical point of view, the stability of finite-size condensates indicates that Oswald ripening is arrested: it was suggested that this could originate from the interplay between phase separation and nonequilibrium chemical reactions [7]. More precisely, in models for active droplets, biomolecular condensates are typically made of proteins that coexist under two states: one in which they tend to form droplets, and one in which they do not. The conversions between these two states are assumed to break detailed balance. This idea, which dates back to the studies of nonequilibrium dissipative structures [8,9], has become prominent in recent theoretical studies and in the context of biomolecular condensates: Flory-Huggins-like continuous descriptions have been designed to account for the formation of active emulsions and chemically active droplets [10–14], and can be engineered experimentally with coacervates [15,16].

However, so far, models of chemically active droplets are spatially continuous and deterministic, in such a way that they cannot account for the polydispersity in size and shape of the droplets. Moreover, these models cannot resolve the dynamics

of the system in the stationary state, where fluctuations are responsible for the continuous nucleation of new droplets, and their coalescence. Both these aspects are crucial at the mesoscale, i.e., when condensates are very small and where thermal fluctuations play a prominent role. Recently, in experiments, this appeared to be a particularly relevant level of description [17]. Additionally, such models rely on the numerical resolution of partial differential equations which are very costly and which then have been limited to 2D systems [10,11,13,14]. In this context, it is mandatory to design particle-based simulations of chemically active droplets. This represents a challenge, both in the understanding of the relevant timescales and microscopic details of the model, and in the interpretation of the data, which requires advanced computational tools.

In this Letter, we propose a microscopic and stochastic model for chemically active droplets. Using Brownian dynamics simulations of model proteins that switch between two states [Fig. 1(a)] and that transiently attract each other [Fig. 1(b)], we identify the conditions under which stable, finite-size droplets may form. The nonequilibrium ingredient of the model is a chemical drive, which breaks detailed balance, and whose amplitude controls the size of the droplets, their polydispersity, and their shape anisotropy [Fig. 1(c)]. In addition, we fully characterize the nonequilibrium steady state, by monitoring the coalescence and shrinkage processes at the level of individual droplets—an aspect out of reach from previous deterministic, coarse-grained descriptions. In this context, the present work reports particle-based simulations of active droplets that form through the interplay between phase separation and chemical reactions which are driven away from equilibrium in a controlled way.

Model. We consider a three-dimensional suspension of Brownian particles made of three species, denoted by A, B, and C. A particles may convert into B, and vice versa—

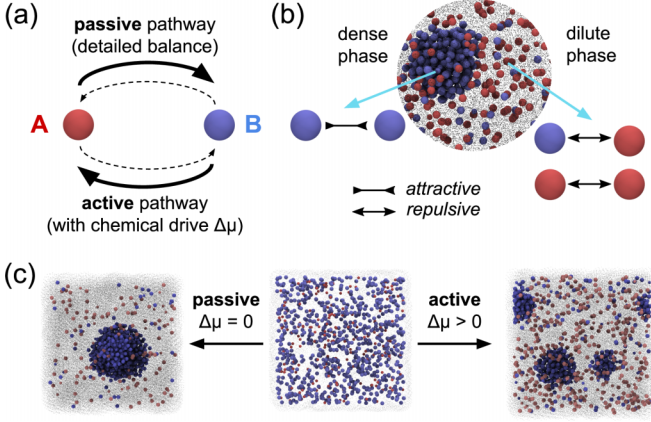[*]These authors contributed equally to this work.

FIG. 1. (a) Two chemical pathways for the interconversions $A \rightleftharpoons B$: a passive pathway, which fulfils detailed balance, and an active pathway, which violates it, because of a constant chemical drive $\Delta\mu$. (b) System under study: chemically active species (A and B) and inert particles (C, represented as gray dots for readability). See text for details on the interaction potentials. (c) Typical snapshots: starting from the same initial configuration, an equilibrium simulation, where species interconversions only follow the passive pathway ($\Delta\mu = 0$), leads to macroscopic phase separation, whereas a nonequilibrium simulation ($\Delta\mu > 0$) leads to interrupted phase separation and selection of a finite droplet size.

the dynamics of these interconversions will be specified later on. To account for the high density of the intracellular medium [18,19], C particles are crowders that do not undergo any reaction. Their density is chosen in such a way that the total volume fraction is 0.1.

We denote by $S_n(t) \in \{A, B, C\}$ the species of particle n at time t. We assume that the positions of particles $r_1, \ldots, r_N$ obey overdamped Langevin equations (see the Supplemental Material [20] for details on the numerical methods [21,22]). The pair interaction between two particles m and n, denoted by $U_{S_n S_m}(r_{mn})$, depends on their species and on their relative distance $r_{mn} = |r_m - r_n|$. The evolution equations of the particles positions read,

$$\frac{dr_n}{dt} = \sqrt{2D}\eta_n(t) - \frac{D}{k_B T}\sum_{m \neq n}\nabla U_{S_n, S_m}(r_{mn}), \quad (1)$$

where we assume that all the particles have the same bare diffusion coefficient D, and where $\eta_n(t)$ is a Gaussian white noise of zero average and unit variance $\langle \eta_{n,i}(t)\eta_{m,j}(t')\rangle = \delta_{ij}\delta_{nm}\delta(t - t')$. Since the dynamics is overdamped, the velocities of the particles at a given time are irrelevant, and the state of the system is completely described by the configuration vector $\mathcal{C} = (r_1, \ldots, r_N; S_1, \ldots, S_N)$. The B particles interact with each other through a Lennard-Jones (LJ) potential, which is truncated at a distance $r_c = 2.5\sigma$ (σ being the diameter of the particles), and shifted in order to ensure continuity of the potential at $r = r_c$. It reads $U_{B,B}(r) = [U_\varepsilon(r) - U_\varepsilon(r_c)]\theta(r_c - r)$, where $U_\varepsilon(r) = 4\varepsilon[(\frac{\sigma}{r})^{12} - (\frac{\sigma}{r})^6]$ is the standard LJ potential and $\theta(r)$ denotes the Heaviside function. All the other pair interactions are purely repulsive and are modeled by the Weeks-Chandler-Andersen (WCA) potential [23], which is simply a Lennard-Jones potential truncated

and shifted at $r = 2^{1/6}\sigma$: $U_{A,\{A,B,C\}} = U_{C,\{A,B,C\}} = [U_{\varepsilon'}(r) + \varepsilon']\theta(2^{1/6}\sigma - r)$. The energy parameters of the interaction potentials are $\varepsilon' = k_B T$ and $\varepsilon = 2k_B T$: the latter ensures that, in the absence of species interconversion, the B particles phase separate at the considered density. Throughout the paper, the distances will be measured in units of σ, the energies in units of $k_B T$, and times in units of σ^2/D.

In order to specify the rules of species interconversions, let us consider two configurations $\mathcal{C}$ and $\mathcal{C}'$, which only differ by the species of one particle. We assume that the species of each particle obey a random telegraph process [24], in such a way that the probability for the system to be in configuration $\mathcal{C}'$ at time $t + \delta t$ knowing that it was in configuration $\mathcal{C}$ at time t reads, for a sufficiently small δt, $P(\mathcal{C}', t + \delta t | \mathcal{C}, t) \simeq k_{\mathcal{C},\mathcal{C}'}\delta t$, where $k_{\mathcal{C},\mathcal{C}'}$ is the rate at which the transition takes place. A crucial feature of our model is that the transition rates have two contributions: a passive one $k_{\mathcal{C},\mathcal{C}'}^p$, and an active one $k_{\mathcal{C},\mathcal{C}'}^a$, in such a way that $k_{\mathcal{C},\mathcal{C}'} = k_{\mathcal{C},\mathcal{C}'}^p + k_{\mathcal{C},\mathcal{C}'}^a$.

First, when the system is at equilibrium, interconversions take place through a "passive" pathway. The conversion rates must obey the detailed balance condition: $k_{\mathcal{C}',\mathcal{C}}^p / k_{\mathcal{C},\mathcal{C}'}^p = \exp\{-\beta[E(\mathcal{C}) - E(\mathcal{C}')]\}$, where $\beta = (k_B T)^{-1}$, and where $E(\mathcal{C}) = \frac{1}{2}\sum_{m \neq n} U_{S_n S_m}(r_{mn}) + \sum_n w_{S_n}$, with w_{S_n} being the internal energy of a particle of species S_n. Second, we consider the situation where detailed balance is broken, and where interconversions take place through an "active" pathway. In this situation, we write the ratio between the rates as $k_{\mathcal{C}',\mathcal{C}}^a / k_{\mathcal{C},\mathcal{C}'}^a = \exp\{-\beta[E(\mathcal{C}) - E(\mathcal{C}') + \kappa_{\mathcal{C}',\mathcal{C}}\Delta\mu]\}$, where $\Delta\mu$ is a chemical drive, and $\kappa_{\mathcal{C}',\mathcal{C}} = 1$ if the transition from $\mathcal{C}'$ to $\mathcal{C}$ implied the formation of a B particle and -1 otherwise (the reason for this choice will be made clear in the next paragraph). The active pathway can be interpreted as follows, if we consider for example the common involvement of ATP in biochemical reaction: if the formation of an A particle is only possible by ATP consumption ($B + \text{ATP} \rightleftharpoons A + \text{ADP}$) and assuming that the chemical potentials of ATP and ADP are almost constant (i.e., they are chemostatted), the chemical drive is actually given by the difference between the chemical potentials of chemostatted species: $\Delta\mu = \mu_{\text{ATP}} - \mu_{\text{ADP}}$ [25].

To form stable droplets, and to avoid the formation of a single one, the formation of A particles must be favored in dense regions (i.e., where droplets tend to form), and, on the contrary, the formation of B particles must be favored in dilute regions. Following the idea from Refs. [7,11,12], we assume that $k_{\mathcal{C}',\mathcal{C}}^p = k_0(1 - \phi_{\text{loc}}/\phi_{\text{max}})e^{-\frac{\beta}{2}[E(\mathcal{C}) - E(\mathcal{C}')]}$ and $k_{\mathcal{C}',\mathcal{C}}^a = k_0(\phi_{\text{loc}}/\phi_{\text{max}})e^{-\frac{\beta}{2}[E(\mathcal{C}) - E(\mathcal{C}') + \kappa_{\mathcal{C}',\mathcal{C}}\Delta\mu]}$, where ϕ_{loc} is the local density of A and B particles around the particle whose species change between configuration $\mathcal{C}$ and $\mathcal{C}'$, and where ϕ_{max} is the maximum volume fraction of the mixture and is approximated to the maximum packing fraction in three dimension: $\phi_{\text{max}} \simeq 0.74$. We fix $k_0 = 10^{-2}$ in all the simulations. With this choice of the reaction rates $k_{\mathcal{C}',\mathcal{C}}^{a,p}$, and at equilibrium ($\Delta\mu = 0$), global detailed balance is fulfilled: $k_{\mathcal{C}',\mathcal{C}}/k_{\mathcal{C},\mathcal{C}'} = \exp\{-\beta[E(\mathcal{C}) - E(\mathcal{C}')]\}$. Therefore, the parameter $\Delta\mu$ controls finely the deviation from equilibrium, as opposed to previous models of mixtures of particles with "active switching", which have been studied in other contexts [26–35]. In those descriptions, the rates of conversion of the particles are independent of their local environment, in
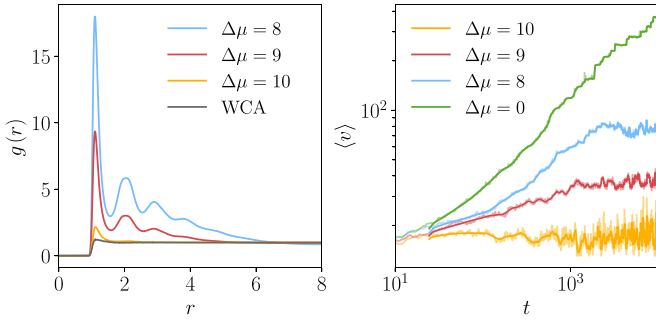
FIG. 2. Left: Radial distribution function (RDF) between $\{A, B\}$ particles in the stationary state (for t between 10^4 and 6×10^4). The RDF for particles in a system at the same density and interacting via a WCA potential is shown in gray for reference. Right: Average volume of the droplets $\langle v \rangle$ as a function of time for various values of the chemical drive $\Delta\mu$. Solid lines are running averages (over 50 points) of the raw data, shown in lighter color.

FIG. 3. Left: Probability distribution of the droplet volume v, for various values of the chemical drive $\Delta\mu$, in the stationary state. The two stars represent, for $\Delta\mu = 8$ and 9, the stable fixed points in the phase portrait shown in Fig. 4. Right: Shape anisotropy of the droplets as a function of their volume v. Solid lines are running averages (over ten points), and the widths of the colored areas are the standard deviations (insets: schematics of the spherical and non-spherical droplets, which correspond, respectively, to low and high values of κ^2).

such a way that the distance of the system to equilibrium is difficult to evaluate.

Another key parameter of our model is the difference between the internal energies $\Delta w = w_B - w_A$. Here, we take $w_A = w_C = 0$ and $w_B = 0.5$, meaning that $\Delta w > 0$, and that A is more stable than B in the absence of interactions. However, stable droplets can also be formed for other choices of Δw (including $\Delta w < 0$). This simply requires to explore other values of the chemical drive $\Delta\mu$. The choice of parameters is discussed in details in the SM, and we show that the formation of stable droplets is not restricted to the parameters shown in the main text [20].

Formation of active droplets. We perform numerical simulations and tune the parameter $\Delta\mu$, which quantifies the deviation from thermal equilibrium, and which will be varied from zero to ten. In the range of parameters we consider, we observe that the B particles tend to form droplets [Figs. 1(b) and 1(c) and movies in the Supplemental Material]. We compute the radial distribution functions of A and B particles, in the stationary state and for $\Delta\mu > 0$ (Fig. 2). These functions bear the signature of the formation of dense clusters that become less structured as $\Delta\mu$ increases. In order to characterize quantitatively the spatial structure, we perform a cluster analysis on each trajectory [20], and compute the average volume of the droplets at time t, denoted by $\langle v \rangle$.

At equilibrium, i.e., when $\Delta\mu = 0$, we observe that $\langle v \rangle$ increases as a power law ($\langle v \rangle \sim t^\alpha$, with $\alpha \simeq 0.48$, see Fig. 2). This slow increase is characteristic of the progressive coarsening of a single droplet, as expected for purely passive systems, through Ostwald ripening. On the contrary, when $\Delta\mu > 0$, one observes that $\langle v \rangle$ quickly saturates at a finite value, that depends on $\Delta\mu$, and that is much smaller than the typical volumes reached at equilibrium (see movies in the Supplemental Material for examples of simulation trajectories). This defines a stationary state in which, although $\langle v \rangle$ does not vary anymore, droplets coalesce and are continuously nucleated in the dilute phase. We then conclude that the active reaction pathway results in droplet size selection, as predicted by continuous-space reaction-diffusion theories [7,10,11]. Note that for values of $\Delta\mu$ smaller than eight, the typical droplet volume that is selected by the active reaction pathway is
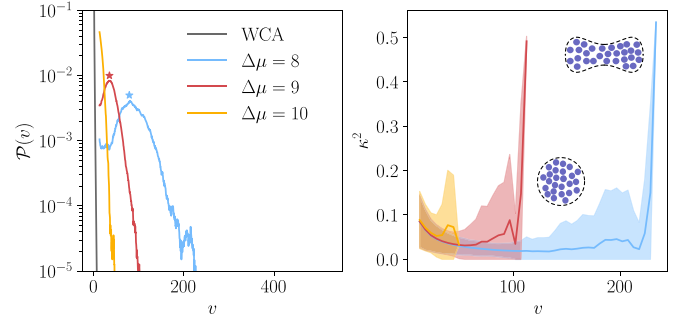
large, and is likely to be comparable to system size, in such a way that strong finite size effects prevent us from reaching stationary state in a reasonable computational time.

Polydispersity and shape anisotropy of the active droplets. As seen in Fig. 2, the volume of the droplets strongly fluctuates around its average value. To quantify the polydispersity of the droplets, we measure the volume of each droplet at each time step and in the stationary state, and we plot the resulting histograms in Fig. 3. For small enough values of $\Delta\mu$, the distributions typically show a wide peak at a large value of v, which represents the volume of the droplet selected by the active pathway. Furthermore, the distribution of v is large, which shows that the droplets are very polydisperse. This is in contrast with purely deterministic approaches, which result in the selection of a single droplet size, with vanishing fluctuations. Finally, we observe that the variances of these distributions decrease as the chemical drive increases.

The probability distribution $\mathcal{P}(v)$ does not contain information about the shapes of the droplets. We characterize them through the computation of the gyration tensors of the droplets and their eigenvalues [20]. We introduce a coefficient κ^2, called shape anisotropy, and that varies between zero and one, which correspond, respectively, to a perfectly spherical droplet and a perfectly elongated one. As seen in Fig. 3, for small enough values of v, the shape anisotropy κ^2 decreases with v: this is expected, as the B particles constituting the droplets arrange in such a way to minimize surface tension. However, for larger values of v, we observe that the shape anisotropy may become an increasing function of the droplets volume. This means that, in this range of parameters, droplets tend to have a more elongated shape than the one that minimizes their surface tension. We interpret this as follows: under the effect of thermal fluctuations, droplets diffuse in the simulation box and coalesce, thus forming large droplets whose shape is elongated (see the inset of Fig. 3 and the movies in the Supplemental Material). Under the combined effect of surface tension and active chemical reactions, droplets that are formed by coalescence events relax to smaller and more spherical droplets. Note that large, aspherical droplets, that result
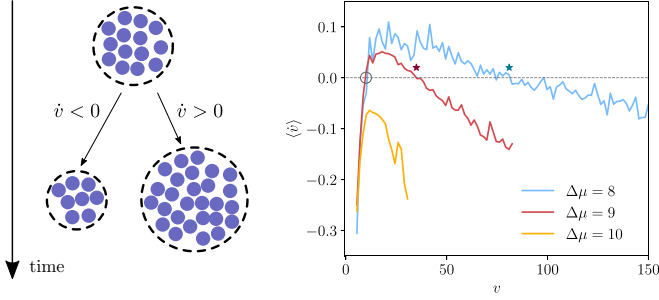
FIG. 4. Left: Schematic representation of $\dot{v}$. Right: Phase portrait of the volume of droplets (derivative of the volume with respect to time as a function of the volume) for different values of the chemical drive $\Delta\mu$. For $\Delta\mu = 8$ and 9, the two stars correspond to the typical volume reached by a droplet (shown on Fig. 3). Open symbol: unstable fixed point. Stars: stable fixed points.

from coalescence events, are quite rare in our simulations and correspond to the tails of the distributions shown on the left of Fig. 3.

Size selection mechanism and lifetime of the active droplets. In order to support this claim, we now study the time evolution of the droplets in the stationary state. Indeed, so far, we have only identified droplets at each timestep without linking them from one step to another. To go further, we design an algorithm to track droplets in time [20]. The volume of each droplet is monitored from its birth (that may occur from spontaneous nucleation) to its death (that may occur through shrinking below a threshold value, or coalescence with another droplet). For each droplet that is then identified and tracked, we compute the derivative of v with respect to time and plot the resulting phase portrait (the average $\langle\dot{v}\rangle$ as a function of v) in Fig. 4.

This plot shows that, for values of the chemical drive that lead to the selection of large droplets ($\Delta\mu = 8$ or 9), the curves cross the horizontal axis twice: there are then two fixed points. First, at small volumes, the unstable fixed point represented by the empty circle in Fig. 4, corresponds to the critical nucleation volume v_{crit}: below this volume, droplets are unstable and dissolve spontaneously. Second, there is a stable fixed point at a volume that we will call v^* and that is represented by the two stars in Fig. 4. We report the values of v^* on the probability distribution shown in Fig. 3 and observe that they correspond to the maxima of $\mathcal{P}(v)$. More precisely, when the droplets have initially a volume between v_{crit} and v^*, the derivative of their volume with respect to time is positive, meaning that they tend to grow by aggregation of B particles from the dilute phase, or coalescence with other droplets. On the contrary, when their initial volume is greater than v^*, $\langle\dot{v}\rangle$ is negative, meaning that they shrink until they reach the stable value v^*.

This mechanism for droplet size selection is therefore a microscopic and stochastic counterpart to the predictions from continuous and deterministic models [10]. In such theories, the typical volume reached by the droplets at equilibrium is understood as a compromise between a growth (resp. loss) term, which dominates at small (resp. large) volumes. However, as opposed to the ideal case considered in those theories (droplets in infinite volume without fluctuations), we cannot
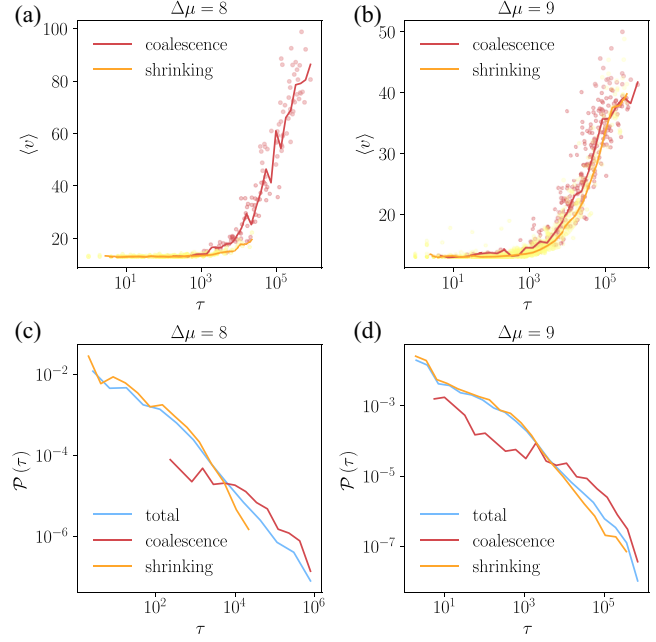

FIG. 5. Average volume of the droplet during its life as a function of the lifetime τ for different death events and for $\Delta\mu = 8$ (a) and $\Delta\mu = 9$ (b). Probability distribution of droplet lifetime τ for different death events and for $\Delta\mu = 8$ (c) and $\Delta\mu = 9$ (d).

identify these terms unambiguously given the limited statistics at small volumes.

Finally, we show that our stochastic simulations capture the broad range of behaviors that emerge in the nonequilibrium steady state. To this end, for each droplet identified and tracked in the trajectories, we compute the number of steps elapsed between its birth and its death [20]—this "lifetime" will be denoted by τ. We observe that there are two reasons for droplets to disappear: they either coalesce with another one or shrink below the critical volume v_{crit}. We show in Figs. 5(a) and 5(b) the average volume of the droplet during their life as functions of their lifetime: the data is split depending on the type of death event. For $\Delta\mu = 8$, large droplets (of volume close to v^*) are very unlikely to shrink below the critical volume v_{crit}: this is consistent with the phase portrait where $v^* \gg v_{\text{crit}}$. As a consequence, they mostly experience coalescence events and their lifetime is much larger then the one of smaller droplets as can be seen on the probability distribution of τ, shown in Fig. 5(c). On the contrary, for $\Delta\mu = 9$, large droplets can either coalesce or shrink: since v^* is closer to v_{crit}, fluctuations can easily bring any droplet below the critical nucleation volume. In this case, the lifetime depends much less on the size of the droplet [Figs. 5(b) and 5(d)]. Interestingly, this shows that the active pathway controls not only the size and shape of the droplets, but also the time during which they persist and keep B particles in close vicinity. This property may play a key role in some biological processes, where condensates are known to act as microscopic "reactors," that bypass the diffusion-limited step of chemical reactions [36,37].

Conclusion. In this Letter, we introduced a particle-based computational framework designed to study active droplets. Our microscopic and stochastic approach enabled us to

simulate Brownian suspensions where Ostwald ripening is interrupted in a controlled way, allowing for a detailed characterization of the polydispersity, shape anisotropy, and fluctuations of active droplets in the nonequilibrium steady state of the system. Our work not only advances the understanding of active emulsions but also provides a versatile methodology applicable to a wide range of systems. As a perspective, the present work opens the way to the understanding of the effect of macromolecular crowding on the formation of biomolecular condensate [38,39].

Data availability. The data that support the findings of this article are openly available [40].

[1] S. F. Banani, H. O. Lee, A. A. Hyman, and M. K. Rosen, Biomolecular condensates: Organizers of cellular biochemistry, Nat. Rev. Mol. Cell. Biol. **18**, 285 (2017).

[2] Y. Shin and C. P. Brangwynne, Liquid phase condensation in cell physiology and disease, Science **357**, eaaf4382 (2017).

[3] A. A. Hyman, C. A. Weber, and F. Jülicher, Liquid-liquid phase separation in biology, Annu. Rev. Cell Dev. Biol. **30**, 39 (2014).

[4] M. Abbas, W. P. Lipiński, J. Wang, and E. Spruijt, Peptide-based coacervates as biomimetic protocells, Chem. Soc. Rev. **50**, 3690 (2021).

[5] B. Gouveia, Y. Kim, J. W. Shaevitz, S. Petry, H. A. Stone, and C. P. Brangwynne, Capillary forces generated by biomolecular condensates, Nature (London) **609**, 255 (2022).

[6] J. Söding, D. Zwicker, S. Sohrabi-Jahromi, M. Boehning, and J. Kirschbaum, Mechanisms for active regulation of biomolecular condensates, Trends Cell Biol. **30**, 4 (2020).

[7] D. Zwicker, The intertwined physics of active chemical reactions and phase separation, Curr. Opin. Colloid Interface Sci. **61**, 101606 (2022).

[8] S. C. Glotzer, D. Stauffer, and N. Jan, Monte Carlo simulations of phase separation in chemically reactive binary mixtures, Phys. Rev. Lett. **72**, 4109 (1994).

[9] J. J. Christensen, K. Elder, and H. C. Fogedby, Phase segregation dynamics of a chemically reactive binary mixture, Phys. Rev. E **54**, R2212 (1996).

[10] D. Zwicker, A. A. Hyman, and F. Jülicher, Suppression of Ostwald ripening in active emulsions, Phys. Rev. E **92**, 012317 (2015).

[11] D. Zwicker, R. Seyboldt, C. A. Weber, A. A. Hyman, and F. Julicher, Growth and division of active droplets provide a model for protocells, Nat. Phys. **13**, 408 (2017).

[12] C. A. Weber, D. Zwicker, F. Jülicher, and C. F. Lee, Physics of active emulsions, Rep. Prog. Phys. **82**, 064601 (2019).

[13] E. Tjhung, C. Nardini, and M. E. Cates, Cluster phases and bubbly phase separation in active fluids: Reversal of the Ostwald process, Phys. Rev. X **8**, 031080 (2018).

[14] N. Ziethen, J. Kirschbaum, and D. Zwicker, Nucleation of chemically active droplets, Phys. Rev. Lett. **130**, 248201 (2023).

[15] K. K. Nakashima, M. H. I. van Haren, A. A. M. André, I. Robu, and E. Spruijt, Active coacervate droplets are protocells that grow and resist Ostwald ripening, Nat. Commun. **12**, 3819 (2021).

[16] K. K. Nakashima, J. F. Baaij, and E. Spruijt, Reversible generation of coacervate droplets in an enzymatic network, Soft Matter **14**, 361 (2018).

[17] F. C. Keber, T. Nguyen, A. Mariossi, C. P. Brangwynne, and M. Wühr, Evidence for widespread cytoplasmic structuring into mesoscale condensates, Nat. Cell Biol. **26**, 346 (2024).

[18] R. J. Ellis and A. P. Minton, Join the crowd, Nature (London) **425**, 27 (2003).

[19] S. B. Zimmerman and A. P. Minton, Macromolecular crowding: Biochemical, biophysical, and physiological consequences, Annu. Rev. Biophys. Biomol. Struct. **22**, 27 (1993).

[20] See Supplemental Material at http://link.aps.org/supplemental/10.1103/PhysRevE.111.L023403 for details on numerical simulations and data analysis and a supplementary movie.

[21] M. P. Allen and D. J. Tildesley, *Computer Simulation of Liquids* (Clarendon Press, Oxford, 1987).

[22] A. P. Thompson, H. M. Aktulga, R. Berger, D. S. Bolintineanu, W. M. Brown, P. S. Crozier, P. J. in 't Veld, A. Kohlmeyer, S. G. Moore, T. D. Nguyen, R. Shan, M. J. Stevens, J. Tranchida, C. Trott, and S. J. Plimpton, LAMMPS - A flexible simulation tool for particle-based materials modeling at the atomic, meso, and continuum scales, Comput. Phys. Commun. **271**, 108171 (2022).

[23] J. D. Weeks, D. Chandler, and H. C. Andersen, Role of repulsive forces in determining the equilibrium structure of simple liquids, J. Chem. Phys. **54**, 5237 (1971).

[24] C. W. Gardiner, *Handbook of Stochastic Methods* (Springer, Berlin, 1985).

[25] F. Jülicher, A. Ajdari, and J. Prost, Modeling molecular motors, Rev. Mod. Phys. **69**, 1269 (1997).

[26] C. A. Brackley, S. Taylor, A. Papantonis, P. R. Cook, and D. Marenduzzo, Nonspecific bridging-induced attraction drives clustering of DNA-binding proteins and genome organization, Proc. Natl. Acad. Sci. USA **110** (2013).

[27] J. Decayeux, V. Dahirel, M. Jardat, and P. Illien, Spontaneous propulsion of an isotropic colloid in a phase-separating environment, Phys. Rev. E **104**, 034602 (2021).

[28] J. Decayeux, M. Jardat, P. Illien, and V. Dahirel, Conditions for the propulsion of a colloid surrounded by a mesoscale phase separation, Eur. Phys. J. E **45**, 96 (2022).

[29] J. Decayeux, J. Fries, V. Dahirel, M. Jardat, and P. Illien, Isotropic active colloids: Explicit vs implicit descriptions of propulsion mechanisms, Soft Matter **19**, 8997 (2023).

[30] H. Alston, A. O. Parry, R. Voituriez, and T. Bertrand, Intermittent attractive interactions lead to microphase separation in nonmotile active matter, Phys. Rev. E **106**, 034603 (2022).

[31] M. Bley, J. Dzubiella, and A. Moncho-Jordá, Active binary switching of soft colloids: Stability and structural properties, Soft Matter **17**, 7682 (2021).

[32] N. Göth, U. Baul, and J. Dzubiella, Active responsive colloids driven by intrinsic dichotomous noise, Phys. Rev. E **106**, 064611 (2022).

[33] M. Bley, P. I. Hurtado, J. Dzubiella, and A. Moncho-Jordá, Active interaction switching controls the dynamic heterogeneity of soft colloidal dispersions, Soft Matter **18**, 397 (2022).

[34] A. Moncho-Jordá and J. Dzubiella, Controlling the microstructure and phase behavior of confined soft colloids by active interaction switching, Phys. Rev. Lett. **125**, 078001 (2020).

[35] T. J. Longo, N. A. Shumovskyi, B. Uralcan, S. V. Buldyrev, M. A. Anisimov, and P. G. Debenedetti, Formation of dissipative structures in microscopic models of mixtures with species interconversion, Proc. Natl. Acad. Sci. USA **120**, e2215012120 (2023).

[36] C. A. Strulson, R. C. Molden, C. D. Keating, and P. C. Bevilacqua, RNA catalysis through compartmentalization, Nat. Chem. **4**, 941 (2012).

[37] M. Castellana, M. Z. Wilson, Y. Xu, P. Joshi, I. M. Cristea, J. D. Rabinowitz, Z. Gitai, and N. S. Wingreen, Enzyme clustering accelerates processing of intermediates through metabolic channeling, Nat. Biotechnol. **32**, 1011 (2014).

[38] A. A. M. André and E. Spruijt, Liquid–liquid phase separation in crowded environments, Int. J. Mol. Sci. **21**, 5908 (2020).

[39] E. Spruijt, Open questions on liquid–liquid phase separation, Commun. Chem. **6**, 23 (2023).

[40] https://doi.org/10.57745/3TVHXV.